Athermal silicon microring electro-optic modulator

Biswajeet Guha,[1] Kyle Preston,[1] and Michal Lipson[1,2,*]

[1]*School of Electrical and Computer Engineering, Cornell University, Ithaca, 14853 New York, USA*

[2]*Kavli Institute at Cornell, Cornell University, Ithaca, 14853 New York, USA*

**Corresponding author: ml292@cornell.edu*

Received March 26, 2012; revised April 17, 2012; accepted April 17, 2012;
posted April 17, 2012 (Doc. ID 165484); published June 6, 2012

We demonstrate a new class of passively temperature stabilized resonant silicon electro-optic modulators. The modulators consist of a ring resonator coupled to a Mach–Zehnder interferometer with tailored thermal properties. We demonstrate 2 GHz continuous modulation over a temperature range of 35 °C and describe the scalability and design rules for such a device.

OCIS codes: 130.4110, 120.6780.

Silicon microring modulators have been proposed as ubiquitous workhorse of future on-chip optical networks [1,2]. The resonant nature of these modulators leads to enhancement of small index changes enabling low power and ultracompact devices. However, precisely the same resonant enhancement also leads to high sensitivity to ambient temperature fluctuations. This fundamental limitation is due to the large thermo-optic (TO) coefficient of silicon (1.86×10^{-4} K^{-1}) [3]. For example, the resonant wavelength of a ring resonator, made out of a 200 nm × 450 nm silicon waveguide, has a sensitivity of 0.11 nm/K, which induces a detuning between the ring resonance and the incident light frequency as temperature changes. For a quality factor of 10,000, the resonance will shift by one linewidth with only 1 °C change in temperature. Note that the typical temperature inside a commercial microprocessor can vary by tens of degrees in a single local hot spot [4], severely limiting the scope of ring-resonator-based modulators.

A variety of approaches have been proposed and successfully implemented to address this high temperature sensitivity; however, most approaches are either power hungry or not compatible with current front end complementary metal-oxide semiconductor (CMOS) microelectronics. Several schemes involving active compensation have been demonstrated, in which heaters provide feedback that dynamically stabilizes the ring resonance [5–8], but these can lead to a significant power overhead. There have also been several schemes that involve passive compensation where polymers with negative TO coefficient counteract the positive TO coefficient of silicon [9–13]. Unfortunately, polymers are not compatible with front end CMOS processes due to reliability and temperature handling issues [10].

In this Letter, we demonstrate a CMOS compatible resonant Si modulator passively temperature compensated by a modified Mach–Zehnder interferometer (MZI). The MZI spectrum blueshifts with temperature to counteract the redshift of a conventional microring resonator [14]. We achieve the unusual blueshift (as opposed to the traditional redshift of silicon photonic devices) by tailoring the degree of optical mode confinement in the silicon waveguides comprising the MZI [14–16]. By delocalizing the mode in one of the arms of the MZI relative to the other, the mode experiences thermal effects of the cladding (SiO_2 in our case), which is significantly different than what the highly localized mode in Si waveguide of the other arm experiences. Reference [17] analyzes such a device in detail. Note that one can also achieve similar behavior by using a slot waveguide in one of the MZI arms [18].

The modified MZI, which compensates the temperature dependence of the ring resonator, is designed by considering the optical paths of the ring and the MZI. The MZI has two sections: in one section, each arm has waveguides of different widths (characterized by differences in their effective mode indices Δn_{eff}) but the same length (L_{mzi}), while, in another section, each arm has waveguides of the same width (characterized by mode effective index n_{eff}) but different lengths (ΔL_{mzi}) (see Fig. 1). The ring resonator is overcoupled to the thinner arm of the MZI. The MZI is balanced, i.e., its interfering optical path lengths are equal to ensure that the overall spectrum is the one of the ring resonator, while its thermal sensitivity is equal and opposite to that of the resonator [17]. The shift in optical paths with temperature of the MZI and the ring are equal when the following is satisfied:

$$\begin{aligned}\text{MZI}(T) &= \left[n_{\text{eff}} + \frac{\partial n_{\text{eff}}}{\partial T} T\right] \Delta L_{\text{mzi}} \\ &\quad + \left[\Delta n_{\text{eff}} + \frac{\partial \Delta n_{\text{eff}}}{\partial T} T\right] L_{\text{mzi}} \\ &= -\left[\frac{\partial n_{\text{eff}}}{\partial T} T\right] 2\pi R, \end{aligned} \tag{1}$$

where R is the ring radius. An athermal ring is then designed by equating coefficients of T and solving Eq. (1) for L_{mzi} and ΔL_{mzi}.

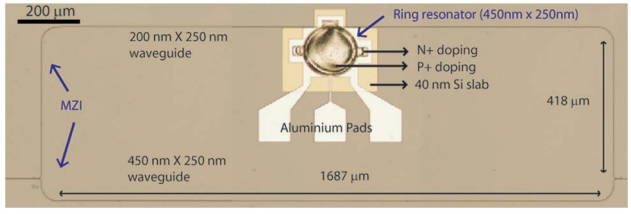

Fig. 1. (Color online) Optical microscope image of the device, which consists of an 80 μm radius ring resonator coupled to an MZI. The ring has a p-i-n diode integrated around it. Waveguide cross sections at various parts of the device are shown.

We fabricate the athermal modulator by integrating a p-i-n diode around the ring resonator, which modulates the phase on one of the arms of the MZI. Thus the modulation scheme remains resonant (which preserves the low power of the modulator), while the MZI acts as a passive thermal stabilization device and translates any phase modulation at the ring into intensity modulation at the output. The devices were fabricated on 250 nm silicon-on-insulator substrate using multiple electron-beam lithography steps. The waveguides were etched using two-step lithography, leaving a 40 nm slab only around the ring for the p-i-n diodes. Next, we performed the implantation steps for the p region (BF_2) and the n region (phosphorous). 1 μm SiO_2 was deposited as a top cladding and multiple annealing steps were performed. Vias were then etched, followed by deposition of contacts and probe pads. Figure 1 shows a microscope image of the final fabricated device. The ring has an 80 μm radius, while the MZI has dimensions of 418 by 1687 μm.The p-i-n diode had a forward resistance of 700 Ω.

We show that the extinction ratio (ER) in our device varies only slightly with temperature and is consistently around 2 dB. Figures 2(a)–2(e) show the normalized optical transmission change at the output, when a CW input laser with 1 μW power was set at the resonance wavelength of the ring (1555.3 nm) and voltage across the diode was swept, for a temperature range of 20–40 °C. The optical power at the output undergoes a transition of around 2 dB for all temperatures for a voltage swing of 1.5 V, indicating that, at every temperature, for a fixed voltage swing, there is a finite modulation in optical transmission. The ER (shown by dotted lines) fluctuates with temperature but does not degrade severely. ER in our devices is mainly limited by the couplers at the input and output of the MZI. This can be easily improved by designing optimized 3 dB couplers. Figure 2(f) shows the theoretical ER dependence with temperature spanning 40 °C. ER decreases just as temperature starts increasing, increases around 10 °C, and decreases somewhat afterward. For an 80 μm radius ring, the temperature period (T_{per}) was 20 °C.

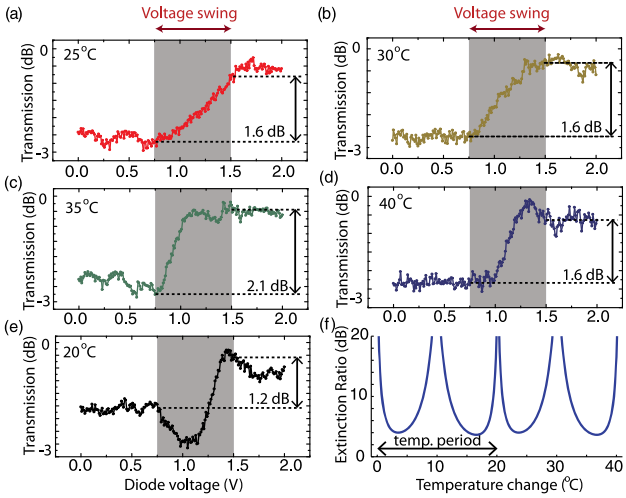

Fig. 2. (Color online) (a)–(e) DC measurement of optical power transition as diode voltage is changed for different temperatures. (f) Change in predicted optical ER with temperature over two temperature periods.

This behavior keeps repeating for higher temperatures. This oscillation of the ER with temperature is due to the fact that, even though the optical path change with temperature of both the MZI and ring can be designed to be equal and opposite, their phases cannot, since the ring phase changes nonlinearly with temperature while the MZI phase changes linearly [17]. We show here that, despite the limitation in the compensation approach, a finite ER is always maintained between the optical ON and OFF states for all temperatures during modulation. In our calculations, we considered a ring with 80 μm radius, n_g (group index) = 4.3, $\Delta n_{\text{eff}}/\Delta T = 1.8 \times 10^{-4}$, 2 dB/cm propagation loss, and a coupling constant of 0.8 to the waveguide. A fixed electron–hole concentration $\Delta N = \Delta P = 1 \times 10^{18}$ cm^{-3} is added to the device, resulting in an effective index shift $\Delta n_{\text{eff}} = -0.003$ and absorption $\Delta\alpha = 14.5$ cm^{-1} [19]. The modulation is assumed to be sufficient to shift the resonance by half of its linewidth. The resonator quality factor is 8000. Note that higher Q factor would cause more asymmetric line shapes, which causes greater degradation of ER with change of temperature, and constrains adjacent channel spacing.

We modulated the applied voltage to the device at 2 gigabits per second (Gbps) and demonstrated open eye diagrams, over a 35 °C temperature range [shown in Fig. 3(b)], which corresponds to two temperature periods. The modulation speed in our devices was limited by the contact resistance. In principle, with optimized p-i-n or p-n diode design, it should be possible to achieve much higher modulation speeds up to tens of gigahertz [1]. Figure 3(a) shows simulated eye diagrams for previously mentioned modulation parameters with a Gaussian noise distribution. One can see that, while there is a periodic change in the shape of the eye with change of temperature, as expected from Fig. 2 due to asymmetric line shapes [17], they remain open. The measured eye diagrams also follow the same pattern [Fig. 3(b)] over a large temperature range.

There is a trade-off between the device area and the temperature operating range for such devices. The fluctuations in ER with temperature increases as the ring radius is reduced due to the corresponding increase in free

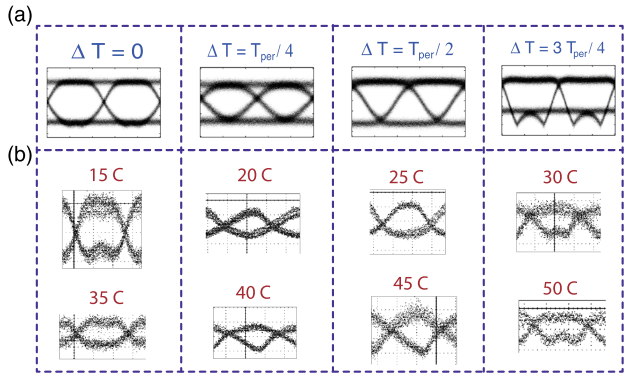

Fig. 3. (Color online) (a) Simulated eye diagrams showing the periodic change in eye diagram shape with temperature over one temperature period. (b) 2 Gbps square wave modulation eye diagrams for different temperatures. Measurements span over two temperature periods. Corresponding predicted eye is shown in the top row.

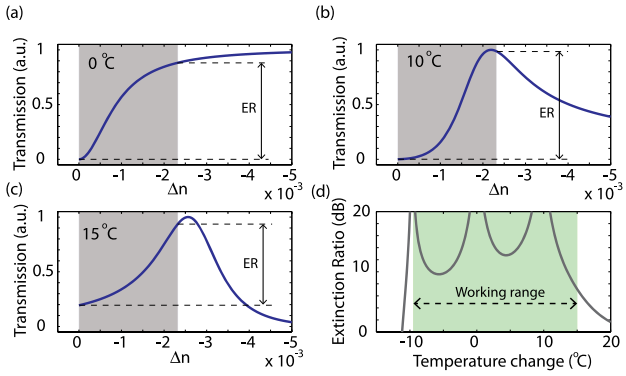

Fig. 4. (Color online) (a)–(c) Optical transmission change as a function of index perturbation of an overcompensated 10 μm radius resonator at different temperatures. ER for a modulation of strength $\Delta n = -2.2 \times 10^{-3}$ is shown. Negative sign indicates resonance blueshift with carrier injection. (d) Change in optical ER with temperature.

spectral range and, therefore, stronger nonlinear dependence of the ring resonator transmission with temperature. This trade-off can be optimized by limiting the working range and using the MZI to overcompensate the thermal redshift of a small ring resonator. In the overcompensated regime, the blueshift of the MZI is stronger than redshift of the ring resonator limiting the detuning in ring resonance, which, in turn, leads to improved ER over a given temperature range. Figures 4(a)–4(c) show the theoretical modulation in optical transmission as a function of index perturbation (negative sign in Δn is due to carrier-injection-based modulation) for different temperatures for a ring with 10 μm radius and $(\Delta \mathrm{MZI}(T)/\Delta T)/\left(2\pi R \frac{\partial n_{\mathrm{eff}}}{\partial T}\right) = -5$ [see Eq. (1)]. All other simulation parameters are the same as mentioned before. One can see that, for three different temperatures, degradation in ER is minimal. Figure 4(d) shows that ER is greater than 3 dB over −10 °C to 15 °C and falls off on either side of these two temperatures. This device has a working range of 25 °C, which is sufficient for most practical applications, and an area approximately 10 times smaller than the device shown in Fig. 1. Note that device area can also be reduced by coiling the MZI arms, limited by the bending radius of the thinner arm.

In conclusion, we showed the first demonstration, to the best of our knowledge, of a silicon microring modulator working over a 35 °C temperature range with no extra power required for thermal stabilization. We presented design procedure and performance analysis of these devices and discussed how to reduce the device footprint. These devices can be custom designed based on the application specifications, and various parameters, such as ring radius, compensation factor, coupling ratio, and mode confinement, can be adjusted to achieve the desired performance. These MZI-assisted resonant athermal devices are naturally suited for wavelength division multiplexing applications since multiple rings can be coupled to the same arm of the MZI, to achieve thermal stabilization. Application of these compact and robust devices can be extended to switching, filtering and other on-chip resonator-based functionalities.

This work is based upon work supported by the National Science Foundation (NSF) under Grants No. 1002060 and No. 1143893. The authors also gratefully acknowledge support from Defense Advanced Research Projects Agency (DARPA) for award No. W911NF-11-1-0435 supervised by Dr. Jagdeep Shah. The devices were fabricated at the Cornell NanoScale Facility (CNF), member of the National Nanotechnology Infrastructure Network (NNIN), which is supported by the NSF.

References

1. G. T. Reed, G. Mashanovich, F. Y. Gardes, and D. J. Thomson, Nat. Photon. **4**, 518 (2010).
2. D. A. B. Miller, Proc. IEEE **97**, 1166 (2009).
3. Y. P. Varshni, Physica **34**, 149 (1967).
4. F. J. Mesa-Martinez, M. Brown, J. Nayfach-Battilana, and J. Renau, in *IEEE International Parallel and Distributed Processing Symposium* (2008), pp. 1–5.
5. C. T. DeRose, M. R. Watts, D. C. Trotter, D. L. Luck, G. N. Nielson, and R. W. Young, in *Conference on Lasers and Electro-Optics*, OSA Technical Digest (CD) (Optical Society of America, 2010), paper CThJ3.
6. P. Dong, R. Shafiiha, S. Liao, H. Liang, N. Feng, D. Feng, G. Li, X. Zheng, A. V. Krishnamoorthy, and M. Asghari, Opt. Express **18**, 10941 (2010).
7. S. Manipatruni, R. K. Dokania, B. Schmidt, N. Sherwood-Droz, C. B. Poitras, A. B. Apsel, and M. Lipson, Opt. Lett. **33**, 2185 (2008).
8. C. Qiu, J. Shu, Z. Li, X. Zhang, and Q. Xu, Opt. Express **19**, 5143 (2011).
9. P. Alipour, E. S. Hosseini, A. A. Eftekhar, B. Momeni, and A. Adibi, Opt. Lett. **35**, 3462 (2010).
10. P. Alipour, A. H. Atabaki, A. A. Eftekhar, and A. Adibi, in *Frontiers in Optics*, OSA Technical Digest (CD) (Optical Society of America, 2010), paper FThQ6.
11. M. Han and A. Wang, Opt. Lett. **32**, 1800 (2007).
12. J. Teng, P. Dumon, W. Bogaerts, H. Zhang, X. Jian, X. Han, M. Zhao, G. Morthier, and R. Baets, Opt. Express **17**, 14627 (2009).
13. V. Raghunathan, W. N. Ye, J. Hu, T. Izuhara, J. Michel, and L. Kimerling, Opt. Express **18**, 17631 (2010).
14. B. Guha, A. Gondarenko, and M. Lipson, Opt. Express **18**, 1879 (2010).
15. M. Uenuma and T. Motooka, Opt. Lett. **34**, 599 (2009).
16. Q. Long, H. Yi, X. Wang, and Z. Zhou, Proc. SPIE **8308**, 83081L (2011).
17. B. Guha, B. Kyotoku, and M. Lipson, Opt. Express **18**, 3487 (2010).
18. X. Tu, J. Song, T. Liow, M. K. Park, J. Q. Yiying, J. S. Kee, M. Yu, and G. Lo, Opt. Express **20**, 2640 (2012).
19. R. A. Soref and B. R. Bennett, IEEE J. Quantum Electron. **23**, 123 (1987).